Engineering Research Express

PAPER • OPEN ACCESS

Low-complexity frequency selective rasorber with polarization-independent switching capability

To cite this article: Zongze Li *et al* 2026 *Eng. Res. Express* **8** 155303

IOP Publishing Eng. Res. Express 8 (2026) 155303 https://doi.org/10.1088/2631-8695/ae8cb2

Engineering Research Express

Check for updates

OPEN ACCESS

RECEIVED
21 October 2025

REVISED
20 May 2026

ACCEPTED FOR PUBLICATION
17 July 2026

PUBLISHED
29 July 2026

PAPER

Low-complexity frequency selective rasorber with polarization-independent switching capability

Zongze Li[1], **Hang Yuan**[2], **Agostino Monorchio**[3], **Danilo Brizi**[3] **and Wenxing Li**[1,*]

[1] The College of Information and Communication Engineering, Harbin Engineering University, Harbin, People's Republic of China
[2] National Key Laboratory on Electromagnetic Environmental Effects and Electro-optical Engineering, Army Engineering University of PLA, Nanjing 210007, People's Republic of China
[3] Department of Information Engineering, University of Pisa, Pisa, Italy
[*] Author to whom any correspondence should be addressed.

E-mail: liwenxing@hrbeu.edu.cn

Keywords: switchable frequency selective rasorber (SFSR), low- complexity, polarization-independent switching capability, dual-transmission band, cost-effective

Abstract

In this paper, a novel low-complexity and cost-effective switchable frequency selective rasorber (SFSR) with polarization-independent switching capability is proposed. To our best knowledge, previously reported electronically reconfigurable and polarization-independent SFSR configurations requires at least 3 distinct layers with no less than 20 SMD lumped components for each unit-cell, causing high cost and fabrication complexity. Conversely, the herein developed switchable rasorber contains only 2 layers with 6 SMD lumped elements for each unit-cell, thus significantly simplifying fabrication and reducing overall cost. To achieve the independent control over TE and TM polarizations, we separate the structure design in perpendicular directions. Two switchable bands are accomplished, whose working mode can be changed from transmission to absorption and reflection to transmission respectively, while only one is usually possessed by previous literature results. By switching the operating state of PIN diodes, the SFSR working mode type is A–T/A–A–R/T. For A–T–A–R mode, it exhibits $S_{11} \leqslant -10$ dB low reflection band of 2.89–8.74 GHz, with 1.17 dB insertion loss. For A–A–A–T mode, it exhibits low reflection band of 3.67–8.2 GHz. Besides, the SFSR has angle stability of 30°. After the design process and numerical simulations evaluation, prototypes are fabricated through PCB technology and characterized in anechoic environment, confirming the overall approach. This work improves about 43% cost effectiveness under same capabilities and it is particularly suitable for all the applications requiring low-complexity and cost-effective fabrication, such as unmanned equipment and antennas radome.

1. Introduction

Frequency selective rasorbers (FSRs) are widely used in radome application and have been received significant research attention from the scientific community. They basically consist in bandpass frequency selective surfaces with out-of-band absorption behaviour, thus reducing the overall radar cross section (RCS) of the enclosed antenna. According to the relative spectrum location of transmission and absorption bands, FSRs can be listed as following types: transmission band below absorption band (T–A) [1–4]; transmission band in between two absorption bands (A–T–A), including single polarization [5, 6], dual polarization [7–9], and broadband [10, 11]; transmission band above absorption region (A-T) [12–14]. Obviously, given a certain transparency band where the enclosed antenna is supposed to operate, the A–T–A type has better performance in terms of RCS reduction.

Although FSR has both transmission and absorption characteristics, its working mode is fixed and its application is limited when facing the increasingly complex electromagnetic (EM) environment. As an evolution of the FSRs, electronically switchable FSRs (SFSRs) recently appeared in the literature. In such deployment, a passive FSR is opportunely equipped with active components that can change their working state upon an electrical signal. When we do not need to transmit signals, we can switch the transmission band to the absorption band or the reflection band to reduce noise or interference. Among the possible solutions to achieve reconfigurability, PIN diodes are the most commonly adopted active components for SFSRs. By starting from the relatively simple SFSRs capable of handling single polarization [5, 15–17], then double polarizations [18–20], and successively double polarizations with independent switching capability [21–23] SFSRs were proposed. The independent switching ability is particularly desirable, since it makes possible to reduce noise in TE (TM) polarization when the SFSR is transparent in TM (TE) polarization. As a matter of fact, achieving such behaviour is relatively complex and, as demonstrated in previous researches on this topic, double polarization with independent switching ability requires at least 3 PCB boards and 20 SMD lumped components to be soldered in each unit-cell. To improve performance of SFSRs, some PCB boards in the exist designs are already multiple layers, which will significantly increase fabrication costs. This is not very favourable for some scenarios that prioritize cost-effective. Besides, they typically have only one transmission band, which limited their applications. A very reduced number of examples about multiple switchable transmission bands can be found in the literature [24] (A–T/R–A–R/T) [25], (A–T–A mode to A–T–A–T–A mode), thus presenting a significant gap. Moreover, a multifunctional metasurface, which can be switched between FSS, absorber, FSR and reflector mode is proposed [26]. Among them, SFSRs contain two functional layers, including 1 lossy layer for absorption and 1 lossy layer for transmission. The lossy layer is designed as a parallel of *LC* and a PIN diode, with an additional *RLC* in series. Based on this circuit mode, extra bias wires are needed to polarize the PIN diodes and affect the resonance of lossy layer. To reduce the influence caused by extra bias wire, it usually needs to solder inductors on bias wire, which also increases fabrication costs.

Therefore, in this paper, we proposed a novel low-complexity and cost-effective SFSR with polarization independent switching ability. In order to reduce complexity and fabrication costs, the proposed SFSR contains only 2 distinct layers, with the lossy one deputed to absorption and the lossless one to allow transmission. To minimize the number of lumped elements, the lossy layer is provided with 2 PIN diodes and 2 resistors to confer the correct resistivity and reactance, while only 2 PIN diodes are soldered in the lossless layer unit-cell. Therefore, fabrication complexity and cost-effectiveness can be significantly improved with just 2 layers and 6 lumped components. In details, polarization independent switching capability is achieved by separating metallic patterns in perpendicular directions. The equivalent circuit model (ECM) is analysed and simulation results are carried out, showing the desired behaviour with two transmission bands for the overall SFSR. By changing the operating state of PIN diodes, one of those band can change the working state between transmission and absorption behaviour, while the other one can change the working state from reflection to transmission. Therefore, the SFSR working mode type is A–T/A–A–R/T. Besides, this paper analyses in detail that the series capacitor of lossy layer is not necessary. Extra biasing wires for polarize PIN diodes of lossy layer also can be removed, which improves cost-effective. Finally, prototypes are fabricated and measured, demonstrating consistency with the numerical results.

The remaining of the paper is organized as follows. Section 2 describes the design and the equivalent circuit analysis of the developed SFSR solution. Section 3 is devoted to compare and discuss numerical and experimental results. Finally, Conclusion will follow.

2. Design and analysis

All the design process and numerical simulations in this manuscript have been carried out by using the numerical solver CST Studio Suite (Dassault Systemes, France) and Advanced design system (ADS, Keysight Technologies, USA).

2.1. Lossy layer design

The lossy layer of the SFSR changes working state enabling transition between absorption and transmission, thus implementing the A–T/A–A type SFSR. The corresponding unit-cell design is shown in figure 1. The substrate is FR-4, with a relative dielectric constant equal to $\varepsilon_r = 4.3$ and a thickness of $h_1 = 0.4$ mm. The copper etching process is the standard 35 μm thick. On the lower right corner of the unit-cell, two metallized via holes allow resistors to be soldered at the bottom side. Electric resonance structures and PIN diodes provide switchable T/A band. The employed PIN diodes are SMP1321-079LF (Skyworks Solutions Inc, USA).

The geometrical design is also analyzed through the Equivalent Circuit Model (ECM), as shown in figure 2(a). $Z_0 = 377\ \Omega$ represent free-space impedance. ECM has been proved a very valuable approach

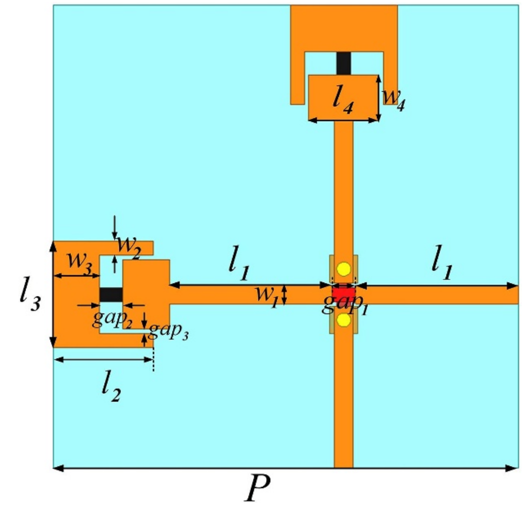

Figure 1. Lossy layer structure. The parameters are listed as follows: $p = 20$ mm, $l_1 = 7$ mm, $l_2 = 4.3$ mm, $l_3 = 4.6$ mm, $l_4 = 3$ mm, $w_1 = 0.8$ mm, $w_2 = 0.6$ mm, $w_3 = 2$ mm, $w_4 = 2$ mm, $gap_1 = 1$ mm, $gap_2 = 1$ mm, $gap_3 = 0.2$ mm.

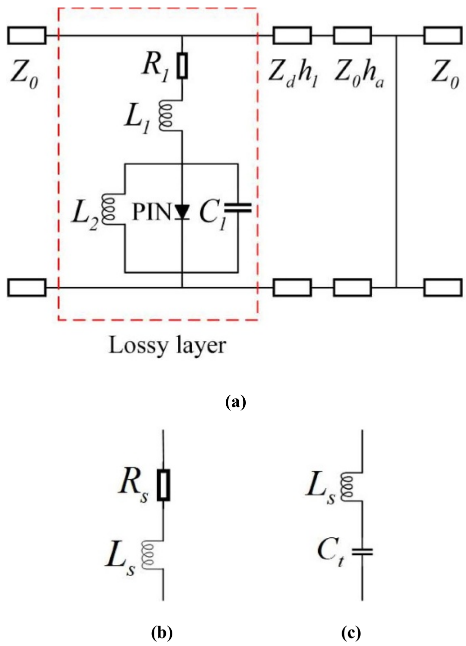

Figure 2. Equivalent circuit model (ECM). (a) Lossy layer. (b) PIN diode 'on' state. (c) PIN diode 'off' state. The parameters are listed as follows: $R = 550\ \Omega$, $L_1 = 9.37$ nH, $L_2 = 1.7$ nH, $C_1 = 0.93$ pF, $R_s = 3\ \Omega$, $L_s = 0.7$ nH, $C_t = 0.1$ pF.

to effectively quantify and control the behaviour of an arbitrarily complex metasurface structure. With regard to our design, PIN diode includes a parasitic inductance L_s in series with a small resistor R_s under 'on' state, as shown in figure 2(b), and a parasitic inductor L_s in series with a capacitance C_t under 'off' state, as shown in figure 2(c).

The inductance can be calculated approximately as follows [31] :

$$L = 2 \times 10^{-7} l \left[\ln\left(\frac{l}{w+t}\right) + 1.193 + 0.2235 \frac{w+t}{l} \right] \tag{1}$$

where l, w and t are the length, width and thickness of the metallic strip.

Instead, the capacitance can be calculated approximately as follows [27] :

$$C = l\varepsilon_0 \varepsilon_e F(k) \tag{2}$$

$$\varepsilon_e = 1 + (\varepsilon_r - 1) F(k)/2F(k_1) \tag{3}$$

$$F(k)=\begin{cases}\frac{1}{\pi}\ln\left(2\frac{1+\sqrt{k'}}{1-\sqrt{k'}}\right), 0<k\leqslant\frac{1}{\sqrt{2}}\\ \frac{1}{\pi}\ln\left(2\frac{1-\sqrt{k}}{1+\sqrt{k}}\right)^{-1}, \frac{1}{\sqrt{2}}<k\leqslant 1\end{cases} \tag{4}$$

where l, w and g are the length, width and distance of the metallic gap, ε_0 is vacuum dielectric constant and ε_{r} is relative dielectric constant of the substrate, thus leading to an average effective value of $\varepsilon_{\mathrm{eff}}=(\varepsilon_r+1)/2$, $k=a/b$, $a=g/2$, $b=a+w$, $k'=\sqrt{1-k^2}$, $k_1=\sinh(\pi a/2h)/\sinh(\pi b/2h)$, .

When PIN diodes operate at 'off' state, by introducing the PIN diode model in figure 2(c) into figure 2(a), the admittance of whole parallel electric resonance structure is:

$$\begin{aligned}Y_{\mathrm{lossy\_off}}&=\frac{1}{j\omega L_2}+\frac{1}{j\omega L_{\mathrm{s}}+\frac{1}{j\omega C_t}}+j\omega C_1\\&=\frac{1-\omega^2(L_2C_1+L_2C_t+L_{\mathrm{s}}C_t)+\omega^4L_2L_{\mathrm{s}}C_1C_t}{j\omega L_2(1-\omega^2L_{\mathrm{s}}C_t)}\\&=\frac{a_1\omega^4+b_1\omega^2+c_1}{j\omega L_2(1-\omega^2L_{\mathrm{s}}C_t)}\end{aligned} \tag{5}$$

where $a_1=L_2L_{\mathrm{s}}C_1C_t$, $b_1=-(L_2C_1+L_2C_t+L_{\mathrm{s}}C_t)$, $c_1=1$..

By imposing $Y_{\mathrm{lossy\_off}}=0$, the transmission frequency $f_{\mathrm{lossy_{off}\_T}}$ can be retrieved:

$$f_{\mathrm{lossy\_off\_T1}}=\frac{1}{2\pi}\sqrt{\frac{-b_1-\sqrt{b_1^2-4a_1c_1}}{2a_1}} \tag{6}$$

$$f_{\mathrm{lossy\_off\_T2}}=\frac{1}{2\pi}\sqrt{\frac{-b_1+\sqrt{b_1^2-4a_1c_1}}{2a_1}}. \tag{7}$$

Besides, the impedance of the entire lossy layer is:

$$\begin{aligned}Z_{\mathrm{lossy\_off}}&=\frac{1}{Y_{\mathrm{lossy\_off}}}+j\omega L_1\\&=\frac{j\omega L_2\left(1-\omega^2L_{\mathrm{s}}C_t\right)}{a_1\omega^4+b_1\omega^2+c_1}+j\omega L_1\\&=\frac{a_1L_1\omega^4+(b_1L_1-L_2L_{\mathrm{s}}C_t)\omega^2+(L_2+c_1L_1)}{a_1\omega^4+b_1\omega^2+c_1}\\&=\frac{a_2\omega^4+b_2\omega^2+c_2}{a_1\omega^4+b_1\omega^2+c_1}\end{aligned} \tag{8}$$

where $a_2=a_1L_1$, $b_2=(b_1L_1-L_2L_{\mathrm{s}}C_t)$, $c_2=L_2+c_1L_1$.

By imposing $Z_{\mathrm{lossy\_off}}=0$, the absorption resonance frequency $f_{\mathrm{lossy\_off\_A}}$ can be retrieved:

$$f_{\mathrm{lossy\_off\_A1}}=\frac{1}{2\pi}\sqrt{\frac{-b_2-\sqrt{b_2^2-4a_2c_2}}{2a_2}} \tag{9}$$

$$f_{\mathrm{lossy\_off\_A2}}=\frac{1}{2\pi}\sqrt{\frac{-b_2+\sqrt{b_2^2-4a_2c_2}}{2a_2}}. \tag{10}$$

Conversely, when PIN diodes operate at 'on' state, by introducing the PIN diode model in figure 2(b) into figure 2(a), the admittance of whole parallel electric resonance structure is:

$$\begin{aligned}Y_{\mathrm{lossy\_on}}&=\frac{1}{j\omega L_2}+\frac{1}{j\omega L_{\mathrm{s}}}+j\omega C_1\\&=\frac{L_2+L_s-\omega^2L_2L_{\mathrm{s}}C_1}{j\omega L_2L_{\mathrm{s}}}.\end{aligned} \tag{11}$$

Similarly, by finding $Y_{\mathrm{lossy\_on}}=0$, the transmission frequency $f_{\mathrm{lossy\_on}}$ can be evaluated:

$$f_{lossy_on}=\frac{1}{2\pi\sqrt{\frac{L_2L_{\mathrm{s}}}{L_2+L_{\mathrm{s}}}C_1}}. \tag{12}$$

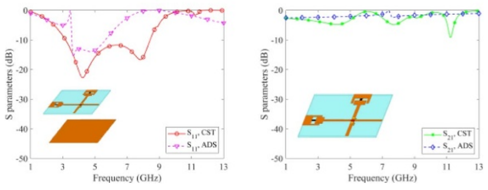

(a) **(b)**

Figure 3. Simulation result of lossy layer. (a) S_{11} parameters of lossy layer with metallic ground plane. (b) S_{21} parameters of lossy layer only.

From equations (6) and (7), by computing the values through the lumped parameters reported in the caption of figure 2, we can obtain: $f_{\text{lossy\_off\_T1}} = 3.8$ GHz, and $f_{\text{lossy\_off\_T2}} = 20$ GHz. Similarly, from equations (9) and (10), we can obtain that even if we remove the series capacitor, we can still obtain the absorption resonance: $f_{\text{lossy\_off\_A1}} = 4.12$ GHz, and $f_{\text{lossy\_off\_A2}} = 20.1$ GHz. Conversely, from equation (12), we can obtain: $f_{\text{lossy\_t}} = f_{\text{lossy\_on}} = 7.4$ GHz. Therefore, we use the 'on' state of PIN diodes as transmission band for our SFSR design, whereas the 'off' state of PIN diodes enabling the corresponding absorption behaviour.

The simulation results of the standalone lossy layer are shown in figure 3. Figure 3(a) compares the S_{11} parameters of lossy layer with metallic ground plane simulated by CST and ADS when PIN diodes operating at 'off' state, while figure 3(b) compares the S_{21} parameters of lossy layer only when PIN diodes working at 'on' state. The results of the two simulation methods show a good degree of consistency to ECM analysis. The obtained absorption extends from 3.17 to 8.42 GHz when the lossy layer has a distance $h_a = 12$ mm with respect to the copper ground. By removing the copper ground, we evaluated the transmission performance of the layer. Thus, when PIN diodes operate at 'on' state, a transmission frequency can be found at $f_{\text{lossy\_on\_sim}} = 6.1$ GHz.

Usually, lossy layers of SFSRs are designed by a parallel of LC and a PIN diode, with an additional RLC in series. This paper indicates that the series capacitor is not necessary. When working frequency is higher than resonance frequency of parallel structure, the parallel structure behaviours as a capacitor, which can provide absorption resonance with series resistor and inductor. When working frequency is lower than resonance frequency of parallel structure, the parallel structure behaviours as an inductor, which will weaken absorption resonance. Therefore, the absorption frequency range is mainly above the resonance frequency of parallel structure. Without series capacitor, we can link the PIN diodes by series, which means that the extra biasing wire for PIN diodes is also not needed. This can reduce the design difficulty caused by extra biasing wires and solve relative undesired effects. However, it is still meaningful to add series capacitor. When working frequency is higher than resonance frequency of parallel structure, adding series capacitor will reduce whole equivalent capacitor of absorption resonance, which will cause the absorption resonance frequency higher. When working frequency is lower than resonance frequency of parallel structure, adding series capacitor will add absorption resonance. Therefore, the series capacitor can extend the absorption band, with the cost of extra bias wire and inductor elements soldered on bias wire, which means higher complexity and cost. In summary, we can remove series capacitor of lossy layer, if we expect cost-effective and a certain extent narrower absorption band.

2.2. Lossless layer design

The lossless layer of SFSR is a switchable FSS (SFSS), as shown in figure 4. The substrate material and thickness as well as the PIN diodes are the same as the lossy layer. On the upper left corner, the copper top layer is linked with the bottom side of SFSS through conductive via holes. Similarly, via holes on the lower right corner of the top layer connected PIN diodes at bottom side of SFSS. The ECM of lossless layer is shown in figure 5. L_3 is an inductor formed by the rectangle structure between the thin metallic strip and the cross gap. L_5 is an inductor root in the cross gap. C_2 is a capacitor stemmed from the cross gap. L_4 is an inductor formed by both the thin metallic strip and the cross gap.

When PIN diodes operate at 'on' state, the admittance of lossless layer is:

$$Y_{\text{lossless\_on}} = \frac{1}{j\omega L_4} + \frac{1}{j\omega L_3 + \frac{1}{j\omega C_2 + \frac{1}{j\omega (L_s + L_5)}}} = \frac{L_3 + L_4 + L_s + L_5 - \omega^2 C_2 (L_3 + L_4)(L_s + L_5)}{j\omega L_4 (L_3 + L_4 - \omega^2 C_2 (L_s + L_5))}. \quad (13)$$

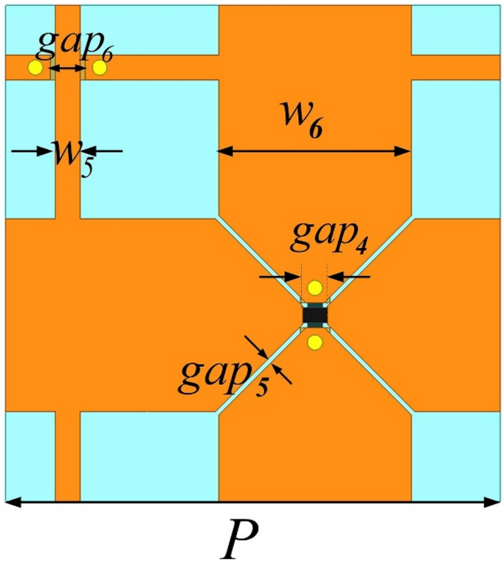

Figure 4. Lossless layer structures. The parameters are listed as follows: $w_5 = 1$ mm, $w_6 = 7.8$ mm, $gap_4 = 1$ mm, $\text{gap}_5 = 0.2$ mm, $\text{gap}_6 = 1.3$ mm.

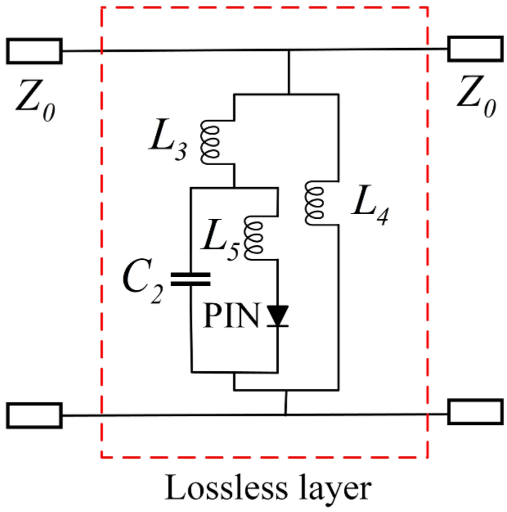

Figure 5. ECM of lossless layer. The parameters are listed as follows: $L_3 = 2.62$ nH, $L_4 = 12.37$ nH, $L_5 = 2.82$ nH, $C_2 = 0.22$ pF.

The transmission frequency $f_{\text{lossless}_o n}$ can be evaluated by imposing $Y_{\text{lossless\_on}} = 0$, as in the following expression:

$$f_{\text{lossless\_on}} = \frac{1}{2\pi\sqrt{C_2\frac{(L_3+L_4)(L_s+L_5)}{L_3+L_4+L_s+L_5}}}. \tag{14}$$

By inserting the lumped values reported in the caption of figure 5 in equation (14), we can obtain that $f_{\text{lossless\_on}} = 6.33$ GHz. It should be pointed out that $f_{\text{lossless\_on}}$ is similar to $f_{\text{lossy\_on}}$. Therefore, we use the 'on' state of PIN diodes at lossless layer to match the 'on' state of PIN diodes at lossy layer. This denotes the low switchable T/A band of the overall SFSR response.

On the other hand, when PIN diodes operate at 'off' state, the lossless layer admittance results:

$$\begin{aligned} Y_{\text{lossless\_off}} &= \frac{1}{j\omega L_4} + \frac{1}{j\omega L_3 + \frac{1}{j\omega(L_s+L_5)+\frac{1}{j\omega C_t}}} \\ &= \frac{a_4\omega^4 + b_4\omega^2 + 1}{j\omega L_4\left(a_3\omega^4 + b_3\omega^2 + 1\right)} \end{aligned} \tag{15}$$

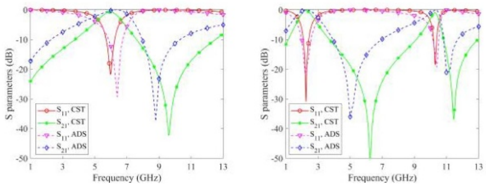

(a) (b)

Figure 6. Simulation results of lossless layer. (a) PIN diodes operate at 'on' state. (b) PIN diodes operate at 'off' state.

where $a_4 = C_2C_t(L_3 + L_4)(L_s + L_5)$, $a_3 = L_3(L_s + L_5)C_t$, $b_4 = -(L_3C_2 + L_3C_3 + L_sC_t + L_5C_t + L_4C_2 + L_4C_t)$, $b_3 = -(L_3C_2 + L_3C_t)$.

In this case, two transmission frequencies of lossless layer, $f_{\text{lossless\_off1}}$ and $f_{\text{lossless\_off2}}$ can be retrieved while $Y_{\text{lossless\_off}} = 0$:

$$f_{\text{lossless\_off1}} = \frac{1}{2\pi}\sqrt{\frac{-b_4 - \sqrt{b_4^2 - 4a_4}}{2a_4}} \tag{16}$$

$$f_{\text{lossless\_off2}} = \frac{1}{2\pi}\sqrt{\frac{-b_4 + \sqrt{b_4^2 - 4a_4}}{2a_4}}. \tag{17}$$

By bring the lumped values reported in the caption of figure 5 in equations (16) and (17), we can get the result that $f_{\text{lossless\_off1}} = 2.27$ GHz and $f_{\text{lossless\_off2}} = 10.33$ GHz. Hence, the higher frequency $f_{\text{lossless\_off2}}$ denotes the switchable R/T band in the upper frequency range of the SFSR response.

As for the lossy layer, we carried out numerical simulations also for the lossless layer in the standalone condition. The corresponding results simulated by CST and ADS are reported in figure 6. The results of the two simulation methods show a good degree of consistency to ECM analysis. When PIN diodes operate at 'on' state, as shown in figure 6(a), a relatively narrowband transmission frequency centred in $f_{\text{lossless\_on\_sim}} = 5.97$ GHz can be observed. Instead, by imposing PIN diodes at 'off' state, as shown in figure 6(b), two transmission frequencies can be identified, one centred at $f_{\text{lossless\_off1\_sim}} = 2.45$ GHz and another in correspondence of $f_{\text{lossless\_off2\_sim}} = 10.27$ GHz. In between these transmission bands a wide reflection band with a very low insertion loss is formed, which can be used as ground of the lossy layer.

As a general observation, from both lossy and lossless layers, we can find that the ECM analysis is more accurate at the lower frequency regime. This happens because the wavelength becomes progressively smaller with the increasing frequencies, and thus the quasi-static hypothesis of unit-cell is less strong. However, the ECM still remains a precious tool to get a physical grasp of the underlined SFSR behaviour.

2.3. Whole SFSR unit-cell design

Basically, the complete SFSR consists of the stacked lossy and lossless layers, separated by a free space gap $h_a = 12$ mm, as shown in figure 7. ECM of the complete SFSR has been retrieved by basically combining the two circuits singularly retrieved in the previous sections and it is reported in figure 8. When PIN diodes at both lossy layer and lossless layer operate at 'on' state, the SFSR works in the A–T–A–R mode. When PIN diodes at both lossy layer and lossless layer operate at 'off' state, the SFSR works in the A–A–A–T mode. Here we simplify the notation of A–T–A–R mode (which also PIN diodes work at 'on' state) into mode 1, and A–A–A–T mode (which also PIN diodes work at 'off' state) into mode 2.

The simulation results are shown in figure 9, for both TE and TM polarizations. When TE and TM polarizations both work at mode 1, as shown in figure 9(a), and mode 2, as shown in figure 9(d), the simulation results of two polarizations are almost the same, which is clear that the SFSR is polarization insensitive. When TE polarization works at mode 1 with TM polarization works at mode 2, as shown in figure 9(b), and TE polarization works at mode 2 with TM polarization works at mode 1, as shown in figure 9(c), it shows different transmission response, which means different polarizations can work at different mode independently. When the SFSR works at mode 1, it exhibits a $S_{11} \leqslant -10$ dB low reflection band coving 2.89–8.74 GHz (100.6%) and a transmission range ($S_{21} \geqslant -3$ dB) at 5.56–6.5 GHz with excellent insertion loss (IL) level equal to 1.17 dB at 6.03 GHz. Conversely, when the SFSR operates at

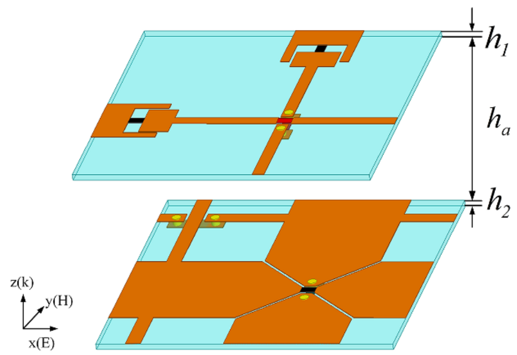

Figure 7. Whole SFSR unit-cell structure.

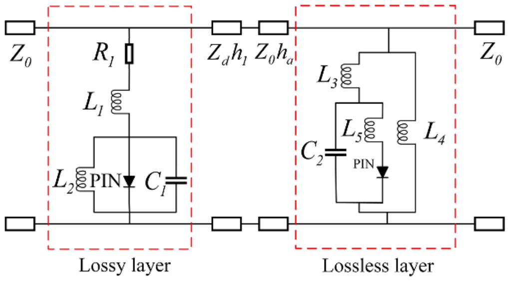

Figure 8. ECM of SFSR.

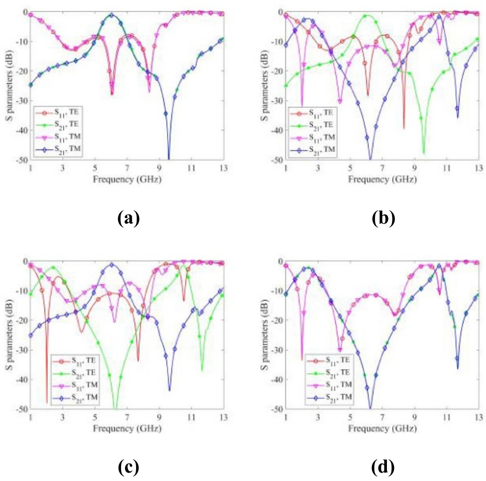

Figure 9. Simulation results of SFSR. (a) TE and TM polarizations both work at mode 1. (b) TE polarization works at mode 1, TM polarization works at mode 2. (c) TE polarization works at mode 2, TM polarization works at mode 1. (d) TE and TM polarization both work at mode 2. *Mode 1: A–T–A–R mode, mode 2: A–A–A–T mode.

mode 2, it exhibits a −10 dB low reflection band coving 3.67–8.2 GHz (76.3%) and a narrow transmission band at 10.53 GHz with a satisfyingly low insertion loss (IL) level of 1.62 dB. We also verified through the simulations of SFSR angular stability, as shown in figure 10 with (a) mode 1 and (b) mode 2. From figure 10(a), we can observe that even with 30° incident angle, it almost has no influence to mode 1. Only transmission centre shifts to 5.89 GHz (3.2%) at 15°. However, the S_{11} parameters change to 7.7 dB for mode 2, weaken absorption characteristic.

In order to present the polarization independence more clearly and explicitly, we run a simulation of surface current when different polarization working at different mode, as shown in figure 11. It shows the result of the proposed SFSR working at 6 GHz, which nears the transmission centre of mode 1. We can observe that the surface current is small of TE polarization operating at mode 1, corresponding to

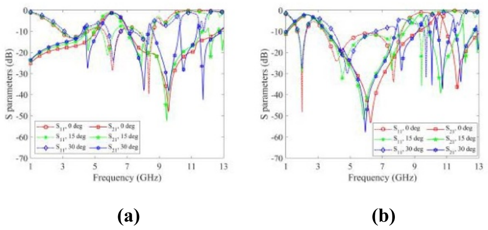

Figure 10. Simulation results of SFSR under oblique incident angle. (a) mode 1. (b) mode 2. *Mode 1: A-T-A-R mode, mode 2: A-A-A-T mode.

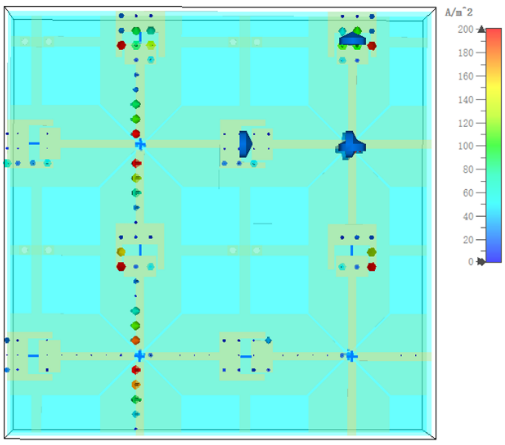

Figure 11. Simulation of surface current at 6 GHz when TE polarization working at mode 1 and TM polarization working at mode 2. *Mode 1: A-T-A-R mode, mode 2: A-A-A-T mode.

transmission resonance. Conversely, the surface current is large of TM polarization working at mode 2, causing energy changing from EM to heat, corresponding to absorption characteristic.

3. Measurement and discussion

3.1. Measure results

A prototype constituted by a 10 × 10 array of the previously described SFSR unit-cell was fabricated through PCB technology and it is shown in figure 12. Figures 12(a) and (b) shows the schematic diagram of measure environment, with S_{11} and S_{21} respectively. Figures 12(c) and (d) show the feeding mode of lossy layer and lossless layer respectively. The overall dimensions of the panel are 235 mm × 235 mm × 12.8 mm. According to the numerical simulations, both the lossy and lossless layers are printed on a 0.4 mm thick FR-4 substrate with plastic support pillar between them. All lumped components are soldered by surface mount technology. As explained in the numerical modelling, one practical advantage of the proposed solution relies on the very simple bias routing required. Indeed, since the PIN diodes of lossy layer are series-connected and PIN diodes of lossless layer are parallel-connected, extra bias wires are not necessary. Standard free space measurement procedure is used to acquire the SFSR S-parameters. In particular, we adopted horn antennas (operating from 2 GHz to 18 GHz, Schwarzbeck) connected to a Vector Network Analyzer (N5245A, Agilent). The distance of the antennas to the SFSR panel is fixed at 1.5 m. The comparisons between measure and simulation results are shown in figure 13, while the angular stability is evaluated in figure 14. Figures 13(a) and (c) show that when SFSR works at mode 1, both TE and TM polarization of the measure results match simulation results well. Figures 13(b) and (d) show the higher transmission band of bith TE and TM polarizations working at mode 2 perform not well. Figure 14 compares the S_{11} and S_{21} parameters between simulation and measurement of mode 1 in (a) and (b) respectively, while S_{11} and S_{21} parameters of mode 2 in (c) and (d) respectively. It shows that the higher transmission band of measurement also does not work well.

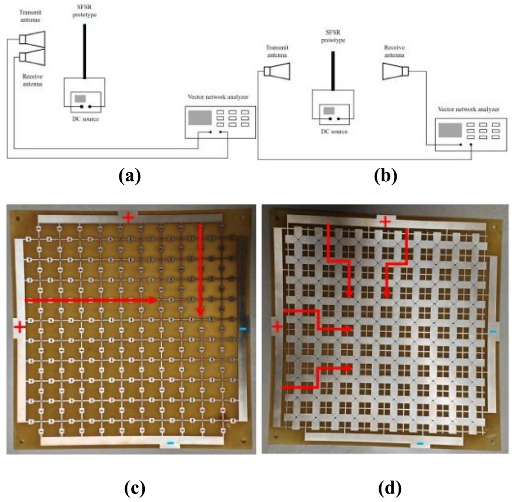

Figure 12. Fabricated prototype of the SFSR in measurement. (a) Schematic diagram of 11 S measure environment. (b) Schematic diagram of 21 S measure environment. (c) Feeding mode of lossy layer. (d) Feeding mode of lossless layer.

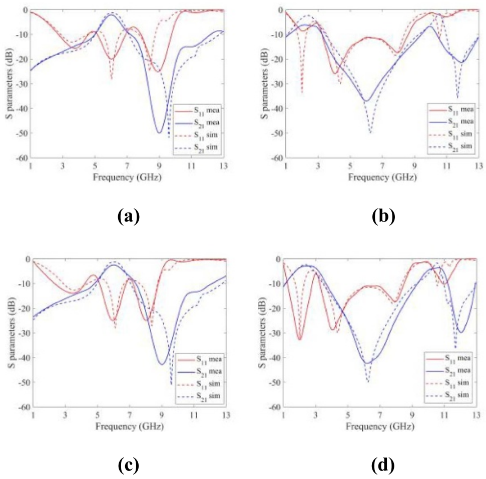

Figure 13. Comparisons between measure results and simulation results. (a) TE polarization working at mode 1. (b) TE polarization working at mode 2. (c) TM polarization working at mode 1. (d) TM polarization working at mode 2. *Mode 1: A–T–A–R mode, mode 2: A–A–A–T mode.

3.2. Discussion

Both figures 13 and 14 show that the transmission results for switchable R/T band in measurement are not so well as simulation results. To analyze this phenomenon, we run simulations of SFSR working at mode 2 with different C_t value, because this value will change under different working frequency, as shown in figure 15. We can observe that when $C_t = 0.075$ pF, transmission band at high frequency range significantly affected. Besides, although the FR-4 substrate is hard plane surface, deformation will also occur when soldering components at high temperatures. These may lead to differences between the measurement and simulation results.

Furthermore, since we remove the series capacitor of lossy layer to avoid extra bias wire and reduce the design complexity, it needs a large voltage to polarize PIN diodes linked in series, especially when the series resistor is large value. Although the PIN diodes we selected can work at ‘on’ state with only 1 mA forward current, the voltage required for the series circuit will also be higher when the sample is larger. In the future, we can replace using resistors to use coding metasurface, which can also be used to reduce RSC [28–30].

Finally, we compared the proposed SFSR performance with the literature in table 1. It can be highlighted that the proposed SFSR needs less layers and lumped elements with respect to other existing multi-functional SFSRs. Together with the simplified bias routing of the PIN diodes, this is a huge advantage in terms of fabrication complexity and cost effectiveness. We compare the SFSRs in literature

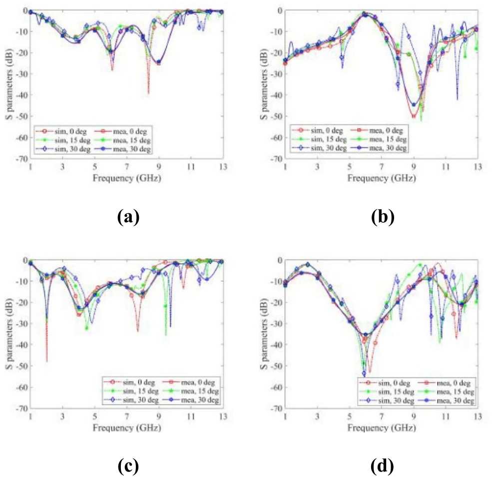

Figure 14. Comparisons of simulation and measure results of SFSR under oblique incident angle. (a) 11 S of mode 1. (b) 21 S of mode 1. (c) 11 S of mode 2. (d) 21 S of mode 2. *Mode 1: A-T-A-R mode, mode 2: A-A-A-T mode.

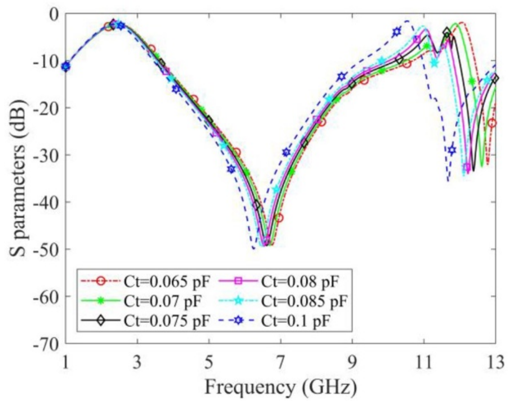

Figure 15. S_{21} simulation results of SFSR working at mode 2 with different C_t. *Mode 2: A-A-A-T mode.

under same dimensions of × 0.5 0.5 m 2, and their fabrication prices are provided by same company. To analyze the cost effectiveness, we define the frequency range that can work at both rasorber mode and absorber mode as the working band of SFSRs. Pri/FBW is used to describe quantitatively of cost effectiveness, and lower Pri/FBW will be more cost effectiveness. Table 1 shows that the proposed design improves about 43% cost effectiveness under same functional capability. Besides, if polarization independently switching capability is not necessary, the proposed design can be designed as single side PCB board for each layer, which will further enhance cost effectiveness. Therefore, the proposed design can be applied to all the practical scenarios requiring such qualities, such as unmanned equipment and antennas radome. In this paper, we simply use Pri/FBW to describe cost-effective. In the future, it may necessary to propose a standard, which combines all performance indicators (such as FBW of absorption, IL, FBW of transmission, and other functional capabilities) to describe cost-effective. This will be conducive to large-scale application.

4. Conclusion

In this paper, we proposed a novel multi-functional SFSR with polarization-independent switching capability, multi-switchable bands and cost effectiveness achieved through an optimized number of SFSR layers and required lumped components. We performed accurate numerical simulations and experimental measurements on fabricated prototypes, confirming the excellent switching capabilities. Moreover, the analysis of the lossy layer indicates that the series capacitor of typically existing designs is not necessary, thus significantly simplifying the biasing wires for PIN diodes. Therefore, this design is characterized by

Table 1. Simulation PERFORMANCE comparison.

	Mode 1			Mode 2							Elements		Price
References	f_t (GHz) IL	Pass band (GHz) FBW	Absorb band (GHz) FBW	Absorb band (GHz) FBW	T (mm) λ_L	AS	P	IS	L	NSB	PIN	all	Pri Pri/FBW
[5]	3.77 0.64	3.5–4.3 20.5%	1.58–5.16 106.2%	1.69–5.04 99.6%	16 0.084	30°	S	N	2	1	3	9	17 222 17 291
[15]	2.88 1.2	2.7–3.01 10.9%	3.9–10.2 89.4%	3.9–10.1 88.6%	9.6 0.092	30°	S	N	2	1	1	5	11 450 12 923
[16]	4 0.4	3.5–4.8 31.3%	0.94–7.2 154%	0.96–6.85 150.8%	41.5 0.118	30°	S	N	3	1	7	12	56 614 37 542
[17]	2.2 1.7	2.16–2.27 4.9%	1.25–2.68 72.7%	1.2–3.7 102%	29.1 0.115	30°	S	N	2	1	4	12	32 060 44 099
[18]	4.28 0.69	NA	2.7–7.8 97.2%	2.8–5.2 60%	15.8 0.137	20°	D	N	2	2	8	12	28 400 47 333
[19]	9.2 0.34	8.8–9.6 8.7%	2.6–7.9 100.9%	2.6–7.9 100.9%	20.6 0.135	40°	D	N	3	1	4	8	56 611 56 106
[20]	5.8 0.45	5.66–5.9 4.1% (−1 dB)	2.9–8.2 90.1%	2.85–8.11 92.6%	8.5 0.082	45°	D	N	2	1	24	28	108 063 119 937
[21]	4.4 0.4	3.6–4.6 14.2% (−1 dB)	0.97–7.43 154%	0.98–6.86 149.9%	38.8 0.124	45°	D	Y	3	1	12	24	80 400 53 636
[22]	4 0.4	3.4–4.5 27.5%	1.4–6 124%	1–8 155.6%	40.5 0.145	30°	D	Y	3	1	12	30	69 838 56 321
[23]	4.1 0.38	3.83–4.86 23.7%	1.34–7.98 142.5%	1.36–7.45 138.3%	35.262 0.15	40°	D	Y	4	1	16	24	344 788 249 304
[26]	NA	4.01–5.83 37%	7.98–12.12 41.2%	8.05–11.93 38.8%	9.916 0.133	45°	D	Y	5	1	16	20	94 356 243 186
This work	6.03 1.17	5.56–6.5 15.6%	2.89–8.74 100.6%	3.67–8.2 76.3%	12.8 0.147	30°	D	Y	2	2	4	6	23 463 30 30751

Mode 1: Rasorber mode in reference papers; Mode 2: Absorber mode in reference papers; FBW: fractional bandwidth; T: Thickness; AS: Angular stability; P: Polarization; IS: Independently switchable; L: Layers; NSB: Number of switchable bands; NA: Not available; Pri: fabrication price of $0.5 \times 0.5m^2$, provided by same company, unit: CHY; Pri/FBW: Cost performance of SFSRs, calculated by Pri divided by minimum FWB (working band of both rasorber and absorber) of SFSR.

fabrication simplicity and improves about 43% cost effectiveness, resulting a perfect match for applications requiring such constraints, as unmanned equipment and antennas radome.

Acknowledgments

The first author thankfully acknowledges the China Scholarship Council for Grant No. 202106680042, supporting his PhD study at University of Pisa from 2022 to 2023.

Data availability statement

All data that support the findings of this study are included within the article (and any supplementary files).

Author contributions

Zongze Li 0009-0005-1229-5744
Formal analysis (equal), Writing – original draft (equal)

Hang Yuan 0000-0002-0435-7440
Data curation (equal), Validation (equal)

Agostino Monorchio 0000-0001-6063-4310
Methodology (equal), Supervision (equal), Writing – review & editing (equal)

Danilo Brizi
Methodology (equal), Writing – review & editing (equal)

Wenxing Li
Conceptualization (equal), Supervision (equal), Writing – review & editing (equal)

References

[1] Filippo C and Agostino M 2012 A frequency selective radome with wideband absorbing properties *IEEE Trans. Antennas Propag.* **60** 2740–7

[2] Motevasselian A and Jonsson B L G 2012 Design of a wideband rasorber with a polarisation-sensitive transparent window *IET Microw. Antennas Propag.* **6** 747–55

[3] Yu W, Luo G Q, Yu Y, Cao W, Pan Y and Shen Z 2019 Dual-polarized band-absorptive frequency selective rasorber using meander-line and lumped resistors *IEEE Trans. Antennas Propag.* **67** 1318–22

[4] Wang Y, Min X, Zhao M, Yuan H, Li R, Hu X and Cao Q 2022 Design of a frequency selective rasorber with a waveform selective passband *IEEE Antennas Wirel. Propag. Lett.* **21** 2125–9

[5] Han Y, Che W, Xiu X, Yang W and Christopoulos C 2017 Switchable low-profile broadband frequency-selective rasorber/absorber based on slot arrays *IEEE Trans. Antennas Propag.* **65** 6998–7008

[6] Sun Z, Chen Q, Guo M, Yu H and Fu Y 2019 Frequency selective rasorber and reflector with two-sided absorption bands *IEEE Access* **7** 6025–31

[7] Chen Q, Sang D, Guo M and Fu Y 2018 Frequency-selective rasorber with interabsorption band transparent window and interdigital resonator *IEEE Trans. Antennas Propag.* **66** 4105–14

[8] Xiu X, Che W, Yang W, Han Y and Xue Q 2020 A highly selective rasorber based on second-order resonance *IEEE Antennas Wirel. Propag. Lett.* **19** 223–7

[9] Bajaj P, Kundu D and Singh D 2022 A dual-polarized L-S-band frequency-selective rasorber with highly selective transmission response *In:. 2022 IEEE Microwaves, Antennas, and Propagation Conf. (MAPCON)* pp 347–51

[10] Yang Y, Liu S, Liao K and Wang L 2022 Design of broadband frequency-selective rasorber with square resonators *2022 Int. Applied Computational Electromagnetics Society Symp. (ACES-China)* pp 1–3

[11] Zhao S, Yang Z, Pang X, Zhang X, Niu M and Fu Y 2022 A broadband frequency selective rasorber with two-sided absorption bands for radome application *In:. 2022 IEEE 5th Int. Conf. on Electronics Technology (ICET)* pp 795–9

[12] Qiang C, Liang C and Jiajun B 2015 Design of absorptive frequency selective surface with good transmission at high frequency *Electron. Lett.* **51** 1596–8

[13] Chen Q, Sang D, Guo M and Fu Y 2019 Miniaturized frequency-selective rasorber with a wide transmission band using circular spiral resonator *IEEE Trans. Antennas Propag.* **67** 1045–52

[14] Zhang H, Ye H, Lu Z, Dai W, Xiao M, Jiang J and Miao L 2022 Miniaturized lossy-layer scheme for designing a frequency selective rasorber *IEEE Antennas Wirel. Propag. Lett.* **21** 2472–6

[15] Bakshi S C, Mitra D and Ghosh S 2019 A frequency selective surface based reconfigurable rasorber with switchable transmission/reflection band *IEEE Antennas Wirel. Propag. Lett.* **18** 29–33

[16] Li R, Tian J, Jiang B, Lin Z, Chen B and Hu H 2021 A switchable frequency selective rasorber with wide passband *IEEE Antennas Wirel. Propag. Lett.* **20** 1567–71

[17] Sun M, Fu X, Guan M, Qin J, Yu Y and Chen A 2023 Impedance-controllable embedded resonator for switchable high-selectivity metamaterial rasorber *IEEE Trans. Microw. Theory Tech.* **71** 3248–58

[18] Yuan J, Kong X, Wang X, Jiang S and Kong L 2020 Polarization-independent reconfigurable frequency selective rasorber/absorber with low-insertion loss *Microw. Opt. Technol. Lett.* **63** 1339–45

[19] Tang M, Zhou D-F, Liu Q-K, Yao Z-N and Liu Q 2021 Low-profile FSS-based polarization-insensitive rasorber with switchable transmission band *IEEE Antennas Wirel. Propag. Lett.* **20** 1038–42

[20] Bakshi S C, Mitra D and Teixeira F L 2021 Wide-angle broadband rasorber for switchable and conformal application *IEEE Trans. Microw. Theory Tech.* **69** 1205–16

[21] Hao J, Shaowei L, Ruiming L and Quan X 2023 Independently switchable rasorber with wide transmission and low-reflection bands under dual polarization *IEEE Trans. Microw. Theory Tech.* **72** 1–15

[22] Jiang B, Hu H, Wu Y, Chen B, Lei S and Tian J 2023 A switchable A-T-A rasorber with polarization selectivity and high roll-off characteristics *IEEE Antennas Wirel. Propag. Lett.* **22** 2075–9

[23] Xiong J, Wu Y, Deng F, Wang K, Yang B, Shi X and Lin H 2026 A dual-polarized frequency-selective rasorber with wideband switchable transmission/absorption capability *IEEE Antennas Wirel. Propag. Lett.* **25** 1547–51

[24] Dong X, He W, Deng K and Chen X 2024 Design of frequency selective rasorber with switchable transmission/reflection bands *2024 Int. Conf. on Microwave and Millimeter Wave Technology (ICMMT)* pp 1–3

[25] Li E, Zhu E, Xiao T, Wang B, Wei Z, Wang Q, Qin F and Yin W-Y 2024 Simultaneous inverse design and uncertainty quantification for frequency-selective rasorber with tunable and switchable abilities by bayesian deep learning *IEEE Trans. Antennas Propag.* **72** 4349–60

[26] Wu Y, Hu H, Tian J, Lei S, Chen B, Wang W and Lin H 2025 A polarization-independent angular-stable active multifunctional metamaterial for amplitude manipulation of electromagnetic waves *IEEE Trans. Microw. Theory Tech.* **73** 3699–709

[27] Gevorgian S and Berg H 2001 Line capacitance and impedance of coplanar-strip waveguides on substrates with multiple dielectric layers pp 1–4

[28] Saleem M, Irfan M, Alanazi M A and Atiq S 2023 2–bit programmable metasurface for low radar cross section antenna and beam steering applications *Radio Sci.* **58** 1-9

[29] Saleem M, Irfan M, Atiq S and Rizwan Anjum M 2023 Low reflection of antenna with wideband reduced backscattered field based on phase interference technique *Phys. Status Solidi a* **220** 2200666

[30] Saleem M, Alanazi M A and Irfan M 2024 A novel broadband low backscattering antenna array based on integration of absorptive and coding metasurface *Microw. Opt. Technol. Lett.* **66** e34358